Antiphasing mechanism of ordered $Ga_{0.5}In_{0.5}P$ layers grown on GaAs (001)

D. Munzar
Laboratory of Thin Films and Nanostructures, Faculty of Science, Masaryk University, Kotlářská 2, 611 37 Brno, Czech Republic

E. Dobročka
Department of Solid State Physics, Faculty of Mathematics and Physics, Comenius University, Mlynská dolina F2, 842 15 Bratislava, Slovak Republic
and Institute of Electrical Engineering, Slovak Academy of Sciences, Dúbravská cesta 9, 842 39 Bratislava, Slovak Republic

I. Vávra, R. Kúdela, and M. Harvanka
Institute of Electrical Engineering, Slovak Academy of Sciences, Dúbravská cesta 9, 842 39 Bratislava, Slovak Republic

N. E. Christensen
Department of Physics and Astronomy, University of Aarhus, DK-8000 Aarhus C, Denmark
(Received 2 May 1997)

$Ga_{0.5}In_{0.5}P$ layers grown by metal-organic chemical-vapor deposition on (001)-oriented GaAs substrates have been studied using transmission electron microscopy. Additional extra diffraction spots found in several projections around the [001] pole and a streaking parallel to the [001] direction observed in the [110] projection are interpreted as due to a laminar structure of the samples consisting of two variants of the CuPt structure with orderings on the $(\bar{1}11)$ and $(1\bar{1}1)$ planes distributed in alternating (001)-oriented laminae. The results of our valence-force-field calculations, including—in an approximate way—the surface reconstruction, suggest a possible origin of the laminar growth. The band-gap reduction of the simplest laminar structures relative to the average gap of the binaries has been calculated by means of the relativistic linear-muffin-tin-orbital method, and found to be significantly lower than that of the CuPt phase. [S0163-1829(98)05607-0]

I. INTRODUCTION

The semiconductor alloy $Ga_{0.5}In_{0.5}P$ is used in optoelectronic devices operating in the visible spectral range. It is almost lattice matched to GaAs, and can thus be easily incorporated into GaAs-based systems.

Since the pioneering work of Gomyo, Suzuki, and Iijima,[1] the $Ga_{0.5}In_{0.5}P$ layers grown on GaAs(001) are known to exhibit long-range order. The ordered structure corresponds to a monolayer superlattice of $(GaP)_1(InP)_1$ in one of the two orientations (variants) $(\bar{1}11)$ and $(1\bar{1}1)$. It will be denoted here for traditional reasons as $CuPt_B$ (or shorter CP_B). The structure is not epitaxially stable,[2] and the surface effects thus have to be considered in order to explain the ordering.

Boguslawski[3] used the valence-force-field (VFF) method[4] to investigate the influence of the surface relaxation. He calculated the energies of different atomic arrangements at the cation-terminated surface and found the one corresponding to the CP_B ordering to be stable with respect to the phase-separated system (Ga plus In). This can be intuitively understood as due to a relatively large number of degrees of freedom of the CP_B surface that can relax to the optimum configuration. However, the calculated value of the magnitude of the the excess energy[5] is rather small (8 meV/surface atom). Bernard, Froyen, and Zunger[6] studied the surface by means of the first-principles pseudopotential method, and showed that it is the electronically driven surface reconstruction consisting of dimerization followed by buckling and tilting of the dimers (*mechanism I*) that stabilizes the CP_B surface over all other forms of surface order. The resulting value of the excess energy (-99 meV/surface atom) is low enough (unlike that obtained by Boguslawski) to account for the ordering of the surface at usual growth temperatures ($\sim$900 K).

In order to explain the experimentally observed large-scale CP_B ordering, it is further assumed[6] that a locally complete cation-terminated surface can form and achieve its optimum arrangement before the subsequent coverage, and that the bulk diffusion following the subsequent coverage cannot alter the established order. In other words, the pattern formed at the surface freezes as soon as it is covered by P atoms.

The above assumption does not yet define the resulting structure: the cation monolayers can be either correlated (bulklike CP_B) or anticorrelated, or something between (see Fig. 1). According to Ref. 3, the cation monolayers should grow in the anticorrelated manner, whereas Ref. 6 suggests that they grow in the correlated pattern. We shall now briefly discuss the arguments which can be used to explain these contradictory results qualitatively. For the sake of simplicity of our explanation, say, that a cation monolayer is of type $C(D)$ if the atomic arrangement corresponds to the CP_B ordering, and is in phase (antiphase) with the arrangement of the first cation monolayer of the alloy. The structure of Fig. 1(a) [Fig. 1(b)] can be described as $CCCCCC$ ($CCDDCC$). Let us consider the growth of a cation monolayer on a C-P-C-P layer (P represents a monolayer of P atoms). The argument of Ref. 3 is as follows. The Ga-P bonds are shorter than those between In and P atoms. The Ga

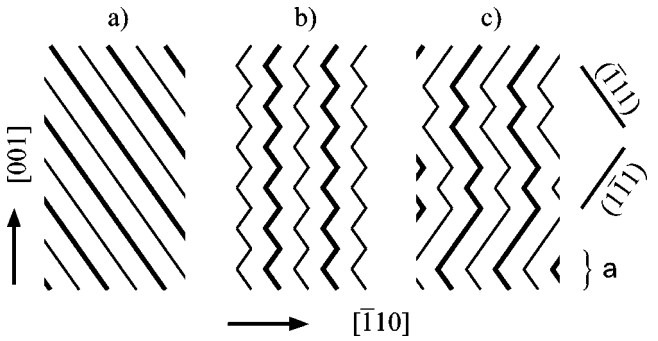

FIG. 1. Schematic diagrams showing (a) correlated, (b) anticorrelated c) irregular stacking of cation monolayers within a layer of ordered $Ga_{0.5}In_{0.5}P$. The thin and thick lines represent planes containing the Ga and In atoms, respectively, and a is the lattice parameter.

(In) atoms are therefore ''looking for'' positions where the P atoms are closer to (farther from) each other. These positions are above those of Ga (In) in the first C monolayer (see Fig. 2 of Ref. 3). That is why the CCD step should appear instead of the CCC pattern corresponding to the three-dimensional (3D) CP_B ordering (antiphasing mechanism). The argument of Ref. 6 is in some sense the reverse. The geometry of the reconstructed cation surface (see Figs. 3, 6, and 14 of Ref. 6) is such that the Ga (In) dimers are very close to (far from) the previous P monolayer. The Ga (In) dimers are thus ''looking for'' positions where the P atoms are farther from (closer to) each other. Consequently, the CCC pattern appears corresponding to the 3D CP_B ordering (phasing mechanism).

The authors of Ref. 6 also considered the case where the cations do not have time enough to form the CP_B order at the surface, and it was shown that the CP_B arrangement can nevertheless arise in the second subsurface cation monolayer (SSCM) below the reconstructed P surface. The P dimers compress the lattice, so that the rows of cations situated below them have less space than the other rows (see Fig. 14 of Ref. 6). If subsurface diffusion occurs at a sufficient rate, the former rows will be occupied by Ga atoms, and the latter rows by In atoms, and the CP_B arrangement will appear (*mechanism II*). The mechanism is, in somewhat simpler form, also presented in Ref. 7. However, as far as we know, the correlation between the cation monolayers in the case of ordering governed by mechanism II has not yet been studied from the point of view employed above, i.e., the surface energetics.

The results of recent TEM studies[8,9] indicate that the samples prepared at temperatures from $\sim$660 to $\sim$750 °C are almost perfect CP_B (the diffraction patterns do not exhibit extra diffraction spots, corresponding to the 3D CP_B ordering) whereas those prepared at temperatures from $\sim$ 520 to $\sim$ 660 °C contain antiphase boundaries (APBS), i.e., such steps as in Figs. 1(b) and 1(c) (the diffraction patterns exhibit streaking parallel to [001], that can be explained as being due to the steps). Other interesting phenomena occur at even lower growth temperatures (see Ref. 12 and references therein). There must be some antiphasing mechanism responsible for the observed loss of correlation at lower temperatures. In case of growth governed by mechanism I, the phasing mechanism of Ref. 6 should dominate, whereas the antiphasing mechanism of Boguslawski is ruled out because it is based on an approach that does not take the surface reconstruction into account. On the other hand, there might be some antiphasing mechanism connected with the growth governed by mechanism II. Our combined experimental and theoretical studies described in this paper suggest such a mechanism.

Results of our TEM studies and their implications for the structure of $Ga_{0.5}In_{0.5}P$ layers are discussed in Sec. II. In Sec. III, we present the results of our VFF calculations, yielding a layer-antiphasing mechanism, and in Sec. IV we discuss the consequences of this mechanism for the fundamental band gap. A short summary is given in Sec. V. Preliminary results of the TEM studies were published in Ref. 10.

II. EXPERIMENTAL RESULTS AND STRUCTURE

The investigated samples were $Ga_{0.5}In_{0.5}P$ epitaxial layers prepared in a AIX 200 low-pressure metal-organic chemical-vapor deposition equipment on (001)-oriented semiinsulating GaAs substrates. The growth temperature was 640 °C, the total pressure inside the reactor was 20 mbar, and the flow velocity was 2.1 ms^{-1}. Specimens for TEM in the (001) (plane view) as well as the (110) orientation (cross section) were prepared by standard techniques consisting of chemical polishing and ion beam etching. TEM observations were performed in a JEOL 1200 EX microscope operating at 120 kV.

Extra diffraction spots were found in several projections around the [001] pole including the [001] projection itself. The most interesting ones are shown in Fig. 2. The extra spots visible in the projections [001], [$\underline{1}03$], and [$\underline{1}14$] correspond to the following **k** vectors: $(\frac{1}{2},\frac{1}{2},0)$; $(\frac{1}{2},\frac{1}{2},\frac{1}{6})$ and $(\frac{1}{2},\frac{1}{2},\frac{1}{2})$; and $(\frac{1}{2},\frac{1}{2},\pm\frac{1}{4})$, respectively. In Fig. 2(d) an example of the [110] diffraction pattern is shown. It can be seen that, instead of sharp spots at positions $(\mp\frac{1}{2},\pm\frac{1}{2},\mp\frac{1}{2})$ and $(\mp\frac{1}{2},\pm\frac{1}{2},\pm\frac{1}{2})$, extremely extended streaking occurs along the [001] direction. The diffraction pattern is symmetrical, which means that both variants of the ordered CP_B structure [$(\bar{1}11)$ and $(1\bar{1}1)$] are developed within the same diffracting area.

In order to explain the observed diffraction patterns, and especially the nonzero intensities at the positions $(\mp\frac{1}{2},\pm\frac{1}{2},0)$, that are clearly visible in Fig. 2(a) (see also Ref. 11), we theoretically analyzed the diffraction patterns of a large variety of model structures consisting of alternating layers of $(\bar{1}11)$ and $(1\bar{1}1)$ variants stacked in the [001] direction. The thicknesses of the layers belonging to the same variant may be the same or may vary around a certain mean value. In this way, we can obtain regular (periodic) or irregular stackings of the layers. Obviously, there are further—more complicated—possibilities to obtain periodic or irregular stackings where the thicknesses of the layers of one variant are not necessarily the same. The samples rather consist of such stackings as deduced from the diffraction patterns. We restricted ourselves to the simpler structures, for which some interesting results and rules can be obtained.

Model structures of sizes $2a\times2a\times200a$ (a being the lattice parameter) were generated in the way described above. The intensity of the diffracted electrons was calculated within the framework of the kinematical theory of dif-

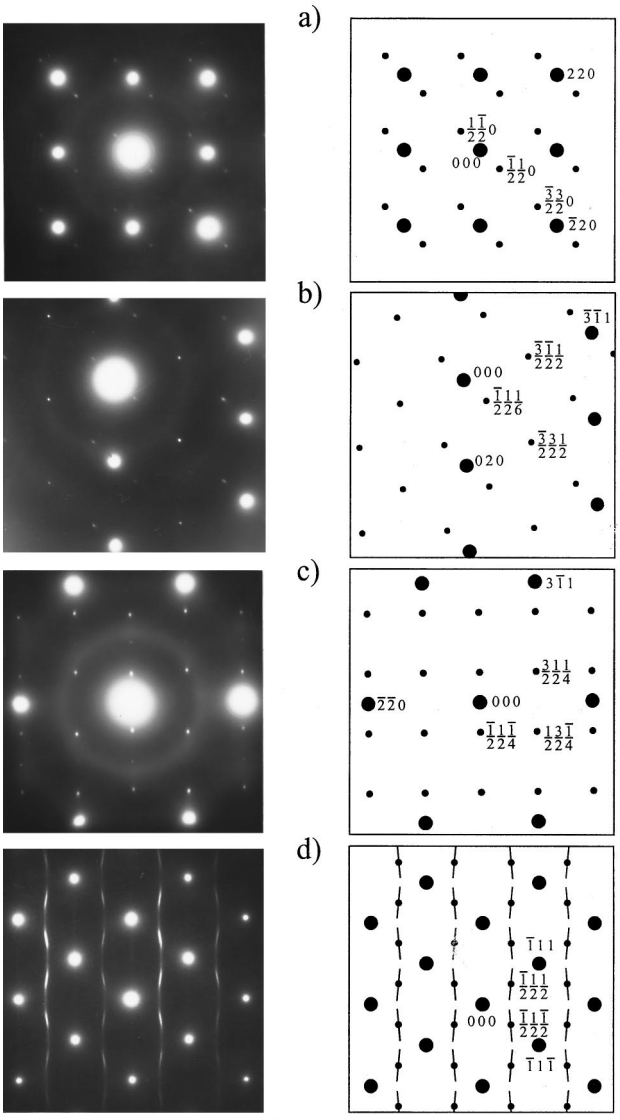

FIG. 2. TEM diffraction patterns of a $Ga_{0.5}In_{0.5}P$ sample obtained in the following projections: (a) [001], (b) [103], (c) [$\bar{1}14$], and (d) [110]. Some rational indices of additional diffraction spots are given in the schematic drawings in the right part of the figure. Large circles—fundamental diffractions; small circles—additional diffractions due to the ordering. In Fig. 4(d), the spots corresponding to the perfectly ordered variants [($\bar{1}11$) and ($1\bar{1}1$)] are marked.

fraction for $k_x=-\frac{1}{2}$, $k_y=\frac{1}{2}$, and k_z varying continuously from $-\frac{1}{2}$ to $\frac{1}{2}$. The size $200a$ in the [001] direction was sufficiently large to give sharp diffraction maxima in the case of periodic structures, and it was suitable for describing an irregular stacking of layers as well.

Examples of the investigated structures are shown in Fig. 3. The structure of Fig. 3(a) represents the simplest case of the periodic stacking of the alternating layers of the two variants, the layers of both variants having the same thickness 1 (in units of $a/2$). This atomic arrangement can be described as $(CCDD)_\infty$ or $(1\text{-}1)_\infty$. The subscript ∞ means a periodic repetition of the pattern described in the parentheses in the [001] direction. The former notation was introduced above, and the latter has the following meaning: the pattern (unit cell) contains a layer of the ($\bar{1}11$) variant and a layer of the

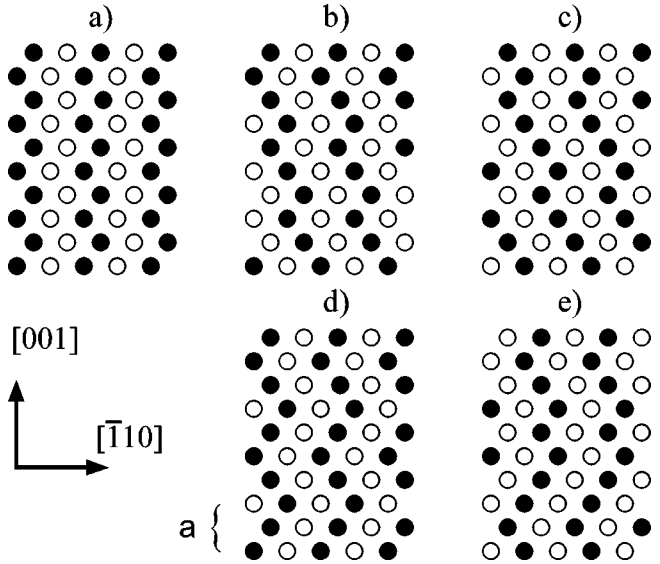

FIG. 3. Schematic diagrams showing the atomic arrangement of some of the investigated structures: (a) (1-1), (b) (2-1), (c) (3-1), and (d) (2-2). (e) Irregular structure. The abbreviations describe the unit cell repeated periodically in the [001] direction. The cell contains a layer of the ($\bar{1}11$) variant and a layer of the ($1\bar{1}1$) variant; the first and the second numbers in the parentheses stand for the number of P monolayers per the former and latter layers. The empty and full circles represent the Ga and In atoms, respectively. The P atoms are not shown.

($1\bar{1}1$) variant; the first and second numbers in the parentheses stands for the number of P monolayers per the former and latter layers. In Figs. 3(b), 3(c), and 3(d), the structures $(CCCDDD)_\infty$ or $(2\text{-}1)_\infty$, $(CCCCDDDD)_\infty$ or $(3\text{-}1)_\infty$, and $(CCCD)_\infty$ or $(2\text{-}2)_\infty$ are shown. Finally, in Fig. 3(e) an example of an irregular stacking of the layers is shown. Note, that the atomic arrangements can be interpreted alternatively as structures containing APB's of high density. For example, the arrangement of Fig. 3(b) can be derived from the ($\bar{1}11$) variant of the CP_B structure generating an APB after every third layer.

All the investigated structures give rise to additional diffraction maxima along the line connecting the points $(\frac{1}{2},\frac{1}{2},\frac{1}{2})$, $(\frac{1}{2},\frac{1}{2},\frac{1}{2})$. For periodic structures, except for the simplest one, the number of these points is larger than 1 and generally, maxima with different k_z-coordinate differ also in intensity. In the case of an irregular stacking of the layers, the intensity is continuously distributed between the points with $k_z=\mp 1/2$. The k_z coordinates corresponding to the additional diffraction maxima of various periodic structures with the layer thicknesses ranging from 1 to 6 (in units of $a/2$) are given in Table I.

Note that there are several structures having their diffraction maxima exactly at the positions visible in the projections used to obtain the patterns of Figs. 2(b) and 2(c): $(2\text{-}1)_\infty$, $(4\text{-}2)_\infty$ and $(3\text{-}1)_\infty$, $(4\text{-}4)_\infty$, $(6\text{-}2)_\infty$, respectively. It is also clear that there is no possibility to unambiguously identify these structures by means of the TEM diffraction analysis.

It can also be seen that, for some structures, the diffraction maxima at the points with $k_z=\pm 1/2$ completely disappear. This is the case of the structures consisting of layers

TABLE I. The k_z coordinates of additional diffraction maxima of various periodic structures with the layer thicknesses ranging from 1 to 6 (in units of $a/2$). The abbreviations of the first and third columns describe the unit cell repeated periodically in the [001] direction. The cell contains a layer of the $(\bar{1}11)$ variant and a layer of the $(1\bar{1}1)$ variant; the first and second numbers in the parentheses stand for the number of P monolayers per the former and latter layers. The maxima are situated along the line connecting the points $(\frac{1}{2},\frac{1}{2},\frac{1}{2})$ and $(\frac{1}{2},\frac{1}{2},\frac{1}{2})$, their third coordinates are given in the second and fourth columns. The number of the maxima is larger than 1 for all the investigated structures, except for the simplest one.

Unit cell	k_z	Unit cell	k_z
(1-1)	0		
(2-1)	$-\frac{1}{2},\frac{1}{6}$	(5-2)	$-\frac{5}{14},-\frac{1}{14},\frac{3}{14},\frac{1}{2}$
(2-2)	$-\frac{1}{2},0,\frac{1}{2}$	(5-3)	$-\frac{3}{8},-\frac{1}{8},\frac{1}{8},\frac{3}{8}$
(3-1)	$-\frac{1}{4},\frac{1}{4}$	(5-4)	$-\frac{7}{18},-\frac{3}{18},\frac{1}{18},\frac{5}{18},\frac{1}{2}$
(3-2)	$-\frac{3}{10},\frac{1}{10},\frac{1}{2}$	(5-5)	$-\frac{2}{5},-\frac{1}{5},0,\frac{1}{5},\frac{2}{5}$
(3-3)	$-\frac{1}{3},0,\frac{1}{3}$	(6-1)	$-\frac{1}{2},-\frac{3}{14},\frac{1}{14},\frac{5}{14}$
(4-1)	$-\frac{1}{2},-\frac{1}{10},\frac{3}{10}$	(6-2)	$-\frac{1}{2},-\frac{1}{4},0,\frac{1}{4},\frac{1}{2}$
(4-2)	$-\frac{1}{2},-\frac{1}{6},\frac{1}{6},\frac{1}{2}$	(6-3)	$-\frac{1}{2},-\frac{5}{18},-\frac{1}{18},\frac{7}{18}$
(4-3)	$-\frac{1}{2},-\frac{3}{14},\frac{1}{14},\frac{5}{14}$	(6-4)	$-\frac{1}{2},-\frac{3}{10},-\frac{1}{10},\frac{1}{10},\frac{3}{10},\frac{1}{2}$
(4-4)	$-\frac{1}{2},-\frac{1}{4},\frac{1}{4},\frac{1}{2}$	(6-5)	$-\frac{1}{2},-\frac{7}{22},-\frac{3}{22},\frac{1}{22},\frac{5}{22},\frac{9}{22}$
(5-1)	$-\frac{1}{3},0,\frac{1}{3}$	(6-6)	$-\frac{1}{2},-\frac{1}{3},0,\frac{1}{3},\frac{1}{2}$

with the thicknesses being odd numbers. More precisely, if the $(\bar{1}11)$ variant is represented by layers with thicknesses 1, 3, 5, . . . , the intensity at the point $(\frac{1}{2},\frac{1}{2},\frac{1}{2})$ (corresponding to a maximum of the $(1\bar{1}1)$ variant) vanishes, because the layers of the $(1\bar{1}1)$ variant are out of phase. The discussions of other possibilities are at hand. This finding is in agreement with the results of Ref. 8, where the microstructure of the ordered structures was widely discussed.

Other interesting problem represents the intensity at $k_z=0$. Our analysis clearly shows that the ''symmetrical'' structures $(1\text{-}1)_\infty$, $(2\text{-}2)_\infty$, $(3\text{-}3)_\infty$, $(5\text{-}5)_\infty$, . . . contribute to the diffraction maximum at $k_z=0$, whereas the remaining symmetrical structures $(4\text{-}4)_\infty$, $(8\text{-}8)_\infty$, . . . do not. In the case of the former structures, the intensity decreases rapidly (although not monotonically) with increasing layer thickness. This is shown in Fig. 4 for layer thicknesses up to 15. A similar behavior was also observed by us in the case of an irregular stacking of layers. Structures consisting of layers with a mean value of the thickness exceeding 10 give practically zero intensity at $k_z=0$.

The results of our simulations along with the experimental observations suggest that the investigated samples consist of alternating layers of the two variants. A considerable intensity at $k_z=0$ indicates that the layers contain only few atomic monolayers.

III. VFF CALCULATIONS AND AN ANTIPHASING MECHANISM

The results presented above provide us with strong evidence of the existence of an antiphasing mechanism. In order to find such a mechanism, we proceed in the following way. We focus our attention on the growth governed by mechanism II, i.e, we assume that the CP_B atomic arrangement arises below the reconstructed P surface in the SSCM. Further, we assume that the atomic arrangement of the cation monolayers situated farther from the surface is frozen. The antiphasing mechanism has to be related to the energy preferences in the SSCM. In order to quantify our considerations, we define the excess energy ΔE_4 corresponding to the SSCM of a given $Ga_{0.5}In_{0.5}P$ layer α terminated by a reconstructed P surface as follows :

$$\Delta E_4[\alpha]=E[\alpha]-\tfrac{1}{2}\{E[\alpha,\ \text{SSCM occupied by Ga atoms}]+E[\alpha,\ \text{SSCM occupied by In atoms}]\}.$$

The lower the value of ΔE_4, the more stable the atomic arrangement in the SSCM. We calculated ΔE_4 for various configurations of the upper two cation monolayers at a fixed configuration of the other cation monolayers using a modified VFF method. In bulk calculations the VFF total energy consists of bond-stretching energies associated with all tetrahedral bonds, and bond-bending energies associated with all pairs of bonds having an atom in common. In this case, however, the VFF treatment of the ''buried'' bonds has to be connected with the surface energetics. Bernard, Froyen, and Zunger[6] did this via matching the pseudopotential-determined geometry of the upper two monolayers with the buried bonds treated by the VFF method, the strain energy of the upper monolayers being neglected. Our approach is less sophisticated but extremely simple: we sum up the contributions of all the III-V bonds including those connecting the surface atoms, and we add the contribution of ''bonding'' energies associated with the P dimers. The latter energies are calculated in the same way as the bond-stretching energies of bulklike bonds. As the equilibrium bond length we adopt the

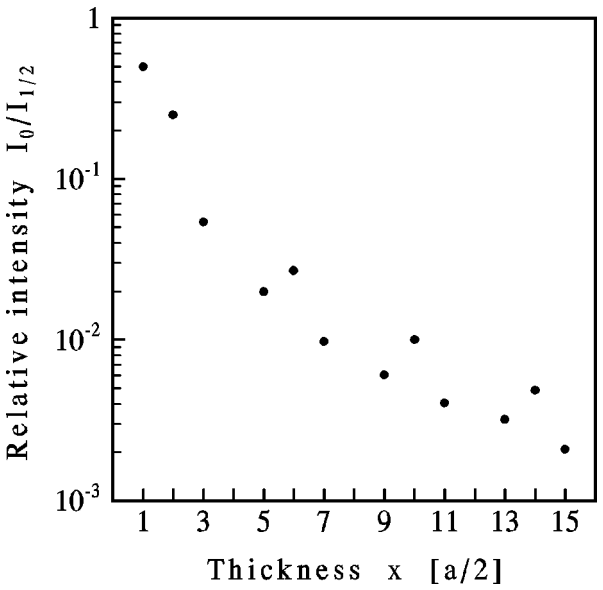

FIG. 4. Relative intensity $I_0/I_{1/2}$ at $k_z=0$ as a function of the thickness x corresponding to the symmetrical unit cell described as $(x\text{-}x)$ repeated periodically in the [001] direction. The values are related to the intensity at the position $k_z=\frac{1}{2}$ calculated for a perfectly ordered $(\bar{1}11)$ variant. Only structures yielding a nonzero intensity are included.

TABLE II. Excess energies ΔE_4 (in meV/surface atom) corresponding to the second subsurface cation monolayer calculated for $Ga_{0.5}In_{0.5}P$ anion-terminated layers grown on GaAs(001). The abbreviations of the first and third columns describe the arrangement of the cation monolayers; the two possible CP_B arrangements are denoted as *C* and *D*, and *A* (*B*) stands for a monolayer consisting of Ga (In) atoms. The last column contains the difference of the energies given in the second and fourth columns.

Structure	ΔE_4	Structure	ΔE_4	Δ
CCDA	−77	*CCCA*	−70	−7
CCDB	−67	*CCCB*	−59	−8
CCDC	−70	*CCCC*	−61	−9
CCDD	−71	*CCCD*	−62	−9
average	−71	average	−63	−8
CCCDC	−70	*CCCCC*	−62	−8
CCDDC	−70	*CCDCC*	−62	−8

distance between P atoms forming a dimer obtained in Ref. 6 (see also Ref. 13). The value of the force constant used in our calculations is 50 N/m. This is our ansatz, that can be justified by two facts. First, the difference between the energies of the *C* and *D* arrangements in the SSCM at fixed position of the P dimers (180 meV/atom) is rather close to the value reported in Ref. 6 (210 meV/atom). Second, the resulting energy differences depend only weakly on the value of the force constant. The values of the force constants of the III-V bonds as well as the lattice parameters were taken from Ref. 14. As unit cells we used the 2×1 surface slabs, the geometry of the upper 7 monolayers (ML) of GaAs and 8 (10) ML of the alloy was relaxed.

The results of our calculations are shown in Table II. The structures of the first column have an APB between the second and third subsurface cation monolayers, whereas those of the third column have not. The large negative values presented in the second and fourth columns confirm the stability with respect to phase separation of the CP_B order in the SSCM. The difference between the excess energies listed in the second and fourth columns is negative, $\sim$ -8 meV, irrespective of the atomic arrangement in the upper cation monolayer. This means that the SSCM will ''prefer'' the arrangement that corresponds to a step with respect to the previous two cation monolayers (antiphasing mechanism). However, the magnitude of the energy difference is rather low, so we can only argue that the steps are more likely to occur than not to occur; the layers should contain steps of 2 ML, but also those of 3 ML and more. This is in good agreement with our experimental findings.

The last two lines demonstrate that the preference for the steps does not depend on the arrangement of the more deeply buried monolayers. This contradicts the empirical ''coincidence structure'' rule introduced in Ref. 8. According to this rule, only such structures can occur for which the number of cation monolayers in any given step is an odd number [the structure of Fig. 3(d) obeys the rule, whereas the structures of Figs. 3(a), 3(b), and 3(c) do not]. If this were so, the arrangement of the deeply buried monolayers would have to influence what is going on in the SSCM, at variance with our results. It can be concluded that either the interpretation of the TEM patterns presented in Ref. 8 is wrong (we expect this is not the case), or that our VFF calculations can give only a partial account of the observed correlations. It is possible that the number of monolayers per step is influenced by the height of surface steps, as suggested in Ref. 15.

The antiphasing mechanism proposed by us is very similar to that of Boguslawski.[3] The qualitative explanation of the latter mentioned in Sec. I can be applied to the growth of the SSCM.

IV. CONSEQUENCES OF THE ANTIPHASING MECHANISM FOR THE FUNDAMENTAL BAND GAP

The CP_B ordering was predicted to cause a significant narrowing (0.46 eV) of the fundamental band gap [band-gap reduction (BGR)] relative to the average over binaries.[16–18] The measured values of the BGR are smaller ($\sim$0.2–0.3 eV depending on the growth conditions, under which the sample has been prepared).[19–22] This discrepancy is usually interpreted[21,22] as due to the fact that the degree of the long-range order η (Ref. 23) of the samples is much lower than 1 (i.e., the ordering of any cation plane is only a partial one). The band gap of the structures grown at lower temperatures could also be strongly influenced by the presence of the APB's. In order to investigate this effect, we calculated the band structures of the superlattices shown in Fig. 3 epitaxially matched to GaAs. The geometries were obtained with the help of the VFF method, that is known to yield accurate estimates of the atomic positions.[24] Note that the calculated equlibrium volumes are smaller by $\sim$ 1% than those obtained by Vegard's rule. Further, in the case of the CP_B structure [$(1\bar{1}1)$ variant], the shift parallel to the substrate surface of each cation monolayer with respect to the previous in the $[\bar{1}10]$ direction is found to be smaller by $\sim$ 3% than that of the ideal zinc-blende geometry. We used the local-density approximation of the density-functional theory and the relativistic linear-muffin-tin-orbital method[25] within the atomic-sphere approximation. We included the empty spheres[26] located at the interstitial tetrahedral sites in order to obtain the close-packed structure, and the so-called combined correction term[25] was included. The calculated conduction bands were shifted toward higher energies by the difference between the experimental (2.07 eV (Ref. 27)) and calculated values of the average gap of the binaries, which is the simplest way to correct for the ''gap problem'' of the local-density approximation. The calculated values of the fundamental band gap are shown in Table III.

The value of the BGR of the CP_B structure (0.39 eV) is somewhat lower than that of Refs. 16 and 17 (0.46 eV), which is probably due to the differences between the computational methods. The values of the BGR corresponding to the other structures are much lower than the former value [with the exception of the (2-2) structure]. This can be interpreted with the help of the zone folding concept. In the case of the CP_B structure, it is the repulsion between the folded zinc-blende Γ and *L* conduction-band states of the ''average crystal,'' that is responsible for the large value of the BGR.[16,17] In the case of the superlattices containing APB's, other zinc-blende states are folded into the Γ point. The interaction between the lowest conduction-band Γ state and

TABLE III. Calculated values of the fundamental band gap ($\Gamma - \Gamma$), E_g, of the GaInP superlattices grown on GaAs (001). The abbreviations of the first column have the same meaning as in Table I. The values in brackets represent the band-gap narrowing.

Unit cell	E_g (eV)
3D CP_B	1.68 (0.39)
(1-1)	1.89 (0.18)
(2-1)	1.87 (0.20)
(3-1)	1.89 (0.18)
(2-2)	1.73 (0.34)

higher folded states is then much weaker than in the former case [that can be easily seen with the help of formula (1) of Ref. 16], and the BGR is thus smaller.

V. SUMMARY AND CONCLUSIONS

Additional extra diffraction spots have been found in several projections around the [001] pole, including the [001] projection itself. Positions of the spots have been compared with those of reciprocal vectors corresponding to simple periodic structures consisting of the two variants of the $CuPt_B$ structure [$(\bar{1}11)$ and $(1\bar{1}1)$] alternating in the [001] direction. In the [110] projection, a streaking parallel to the [001] direction was observed, which was compared with diffraction patterns of periodic and irregular stackings of the two $CuPt_B$ variants obtained by theoretical simulations. The experimental results, especially the nonzero intensity at positions $(\pm\frac{1}{2}\mp\frac{1}{2},0)$, provide reliable evidence that the investigated structures consist of very narrow alternating layers of the two variants. In other words, the ''phase'' of the cation monolayers changes rather frequently.

The VFF method has been used to study the energy preferences in the SSCM below the reconstructed P surface. It is this monolayer, where the ordering probably arises[6] due to the subsurface diffusion. The optimum atomic arrangement has been found to correspond to an APB with respect to previous cation monolayers: an anticorrelated pattern is preferred. The suggested antiphasing mechanism could apply either at lower growth temperatures—this is the case of our samples—or at group-V-rich conditions (see Ref. 19; the results presented therein can be viewed as an indirect evidence of our hypothesis). In both cases the group-III adatoms do not have enough time to achieve their optimum arrangement at the surface.

The calculated values of the fundamental band gap of the simplest laminar structures are higher than that of the $CuPt_B$ structure. The presence of the APB's thus represents one of the reasons (together with the departure of the degree of the long-range order from unity) why the observed band-gap reduction is much lower than the predicted.

ACKNOWLEDGMENTS

D.M. was supported by Grant No. VS96102 of the Ministry of Education of Czech Republic. E.D. was supported by the Scientific Grant Agency of Ministry of Education of Slovak Republic and Slovak Academy of Sciences, Contract No. 1/4319/97. The band-structure calculations were carried out at the Supercomputer-centrum in Brno. We are grateful to Václav Holý for a critical reading of the manuscript.

[1] A. Gomyo, T. Suzuki, and S. Iijima, Phys. Rev. Lett. **60**, 2645 (1988).

[2] J. E. Bernard, L. G. Ferreira, S. H. Wei, and A. Zunger, Phys. Rev. B **38**, 6338 (1988).

[3] P. Boguslawski, Phys. Rev. B **42**, 3737 (1990).

[4] P. N. Keating, Phys. Rev. **145**, 637 (1966).

[5] The excess energy is defined as the difference between the energy of a given cation-terminated layer and the energy of the same layer with the surface monolayer consisting of separated regions of Ga and In.

[6] J. E. Bernard, S. Froyen, and A. Zunger, Phys. Rev. B **44**, 11 178 (1991).

[7] B. A. Philips, A. G. Norman, T. Y. Seong, and S. Mahajan, G. R. Booker, M. Skowronski, J. P. Harbison, and V. G. Keramidas, J. Cryst. Growth **140**, 249 (1994).

[8] C. S. Baxter, W. M. Stobbs, and J. H. Wilkie, J. Cryst. Growth **112**, 373 (1991).

[9] I. Vávra and R. Kúdela (unpublished).

[10] E. Dobročka, I. Vávra, R. Kúdela, and M. Harvanka, in *Heterostructure Epitaxy and Devices*, edited by J. Novák and A. Schlachetzki, Vol. 11 of *NATO Advanced Study Institute, Series 3: High Technology* (Kluwer, Dordrecht, 1996).

[11] The nonzero intensity at these positions should be visible also in Fig. 2(d). This is not the case due to a limited experimental resolution. We have also tried to determine the value of the intensity ratio $I(\bar{\frac{1}{2}},\frac{1}{2},0)/I(\bar{\frac{1}{2}},\frac{1}{2},\bar{\frac{1}{2}})$ using a slow-scan CCD camera. However, our attempts to measure the intensity distribution directly in the TEM failed due to the presence of strong fundamental reflections.

[12] S. B. Zhang, S. Froyen, and A. Zunger, Appl. Phys. Lett. **67**, 3141 (1995).

[13] We use the 2×1 surface cell whereas the authors of Ref. 6 use 2×2 surface cell. Our equilibrium bond length is the average over the two P dimers of Ref. 6.

[14] R. M. Martin, Phys. Rev. B **1**, 4005 (1970).

[15] L. C. Su and G. B. Stringfellow, Appl. Phys. Lett. **67**, 3626 (1995).

[16] S. H. Wei and A. Zunger, Phys. Rev. B **39**, 3279 (1989).

[17] S. H. Wei and A. Zunger, Appl. Phys. Lett. **56**, 663 (1990).

[18] M. E. Raikh and E. V. Tsiper, Phys. Rev. B **49**, 2509 (1994).

[19] M. K. Lee, R. H. Horng, and L. C. Haung, J. Cryst. Growth **124**, 358 (1992).

[20] R. G. Alonso, A. Mascarenhas, G. S. Horner, K. A. Bertness, S. R. Kurtz, and J. M. Olson, Phys. Rev. B **48**, 11 833 (1993).

[21] P. Ernst, C. Geng, F. Scholz, H. Schweitzer, Y. Zhang, and A. Mascarenhas, Appl. Phys. Lett. **67**, 2347 (1995).

[22] M. Schubert, R. Rheinlander, and V. Gottschalch, Solid State Commun. **95**, 723 (1995).

[23] D. B. Laks, S. H. Wei, and A. Zunger, Phys. Rev. Lett. **69**, 3766 (1992).

[24] G. P. Srivastava, J. L. Martins, and A. Zunger, Phys. Rev. **31**, 2561 (1985).
[25] O. K. Andersen, Phys. Rev. B **12**, 3060 (1975).
[26] U. Schmid, N. E. Christensen, and M. Cardona, Phys. Rev. B **41**, 5919 (1990), and references therein.
[27] The value used is the average over the room -temperature band-gap energies presented in *Semiconductors, Physics of Group IV Elements and III-V Compounds*, edited by O. Madelung, M. Schulz, and H. Weiss, Landolt-Börnstein, New Series, Group III, Vol. 17, Pt. a (Springer, Berlin, 1982).